CHAPTER 194

TOTAL RATE AND DISTRIBUTION OF LONGSHORE SAND TRANSPORT

Akira Watanabe[1]

Abstract

Longshore sand transport rate has been computed, for 2,520 cases covering field- and laboratory-scale conditions, using a general formula for local transport rate in a coexistent wave-current field proposed by the present author. The computed total transport rate has been well related to the alongshore component of wave power and two other parameters. Cross-shore distributions of the longshore transport rate have also been studied.

1. Introduction

Longshore sediment transport plays a very important role particularly in long-term beach evolutions. In the longshore transport, sand grains are set in motion mainly by wave action and then carried by a longshore current. However the total transport rate is usually estimated using the CERC formula or its equivalence, which relates the total rate directly with the so-called longshore component of energy flux (or power) of breakers and does not explicitly involve the longshore current velocity. The CERC-type formulas are based on the power or energetics model concept and field measurements, but their reliability and appropriate values of the coefficients are yet debatable. In addition there have been only few studies on the cross-shore distribution of the local transport rate, which is regarded as important as the total rate for various engineering problems.

Watanabe *et al.* (1986) have proposed a power-model type formula for local sediment transport rate under combined action of waves and currents, whose validity has been confirmed through numerous fundamental studies and practical applications (*e.g.*, Watanabe *et al.*, 1991). This local transport rate formula

[1] Professor, Dept. of Civil Eng., Univ. of Tokyo, Bunkyo-ku, Tokyo, 113 Japan.

is applied in the present paper to the evaluation of the total rate and cross-shore distribution of the longshore sand transport under regular waves on straight beaches.

2. Computational Procedure for Waves, Currents and Sand Transport

2.1 Computational conditions

From the standpoint of such fundamental studies as this, computation of waves, currents and sediment transport should be performed for conditions as simple as possible. It has therefore been assumed in the following computation that the shoreline and depth-contour lines are straight and parallel to each other, that incident waves are regular and uniform in the alongshore direction, and that the sediment grain size is spatially uniform. On the other hand, for the sake of generalization of discussions, the computation has been conducted for a total of 2,520 cases: six values of the sand grain diameter d, four values of the uniform bottom slope $\tan\beta$ and a bar-type beach, and three, seven and eight values of the incident wave angle θ_0, period T and height H_0, respectively, as shown in Table 1, covering field- as well as laboratory-scale conditions.

Table 1 Computational conditions.

d (mm)	$\tan\beta$	θ_0 (deg)	T (s)	H_0 (m)
0.2	1/10		1.0	0.02
		15		0.04
0.5	1/20		1.5	0.08
0.8			2.0	0.16
1.1	1/30	30	6.0	0.3
1.5	1/50		10.0	0.6
		45	14.0	1.2
2.0	bar-type		18.0	2.4

2.2 Computation of nearshore waves

A set of time-dependent mild-slope equations, proposed by Watanabe and Maruyama (1986) and improved by Watanabe and Dibajnia (1988), can deal with most of nearshore wave deformation such as shoaling, refraction, reflection, diffraction, breaking and recovery. For the present problem, we can reasonably neglect the wave reflection from the shore and the refraction due to the presence of currents, and then the time-dependent mild-slope equation set reduces to the following simple wave energy equation:

$$\frac{\mathrm{d}}{\mathrm{d}x}(H^2 C_g \cos\theta) = -n f_{\mathrm{D}} H^2 \tag{1}$$

where x is the shoreward coordinate, H is the wave height, C_g is the group velocity, θ is the wave angle, and n is the shallowness factor. The quantity f_{D} is the breaker-induced energy dissipation factor and defined as:

$$f_{\mathrm{D}} = \frac{5}{2}\tan\beta\sqrt{\frac{g}{D}}\sqrt{\frac{(H/D)-\gamma_r'}{\gamma_s'-\gamma_r'}} \tag{2}$$

$$\gamma_s' = 0.8\,(0.57 + 5.3\,\tan\beta), \quad \gamma_r' = 0.4\,(H/D)_{\mathrm{B}} \tag{3}$$

in which $D = h + \eta$ is the local mean water depth (h: the still water depth; η: the mean water surface elevation), and the suffix B indicates the breaking point. Equation (1) has been solved together with Snell's law and Eq. (4) for the wave setup/down to obtain cross-shore distributions of the mean water depth D, wave height H, wave angle θ, group velocity C_g, and so on.

$$\frac{\mathrm{d}\eta}{\mathrm{d}x} = -\frac{1}{\rho g D}\frac{\mathrm{d}S_{xx}}{\mathrm{d}x} \tag{4}$$

where S_{xx} is the normal component of the radiation stress, and ρ is the water density. The location of wave breaking has been determined using a generalized breaker index expressed in terms of the ratio of the horizontal orbital velocity at the wave crest to the wave celerity (Watanabe *et al.*, 1984).

2.3 Computation of longshore current

Since the wave field is stationary and uniform in the alongshore direction, the longshore current velocity has been computed by the following equation (Nishimura, 1988):

$$\rho\, C_{\mathrm{f}}\, \tilde{W}\, V_\ell - \frac{\mathrm{d}}{\mathrm{d}x}\left[\mu_e D \frac{\mathrm{d}V_\ell}{\mathrm{d}x}\right] + \frac{\mathrm{d}S_{xy}}{\mathrm{d}x} = 0 \tag{5}$$

where

$$\left.\begin{aligned} \tilde{W} &= W + (\tilde{u}\cdot\sin\theta)^2/W, \quad \tilde{u} = (2/\pi)\,\hat{u}_b \\ W &= \left[\sqrt{V_\ell^2 + \tilde{u}^2 + 2\,V_\ell\,\tilde{u}\sin\theta} + \sqrt{V_\ell^2 + \tilde{u}^2 - 2\,V_\ell\,\tilde{u}\sin\theta}\right]/2 \end{aligned}\right\} \tag{6}$$

$$\mu_e = \rho N \xi \sqrt{gD} \tag{7}$$

in which V_ℓ is the longshore current velocity, C_{f} is the friction coefficient for the current, S_{xy} is the tangential radiation stress, $\hat{u}_b$ is the near-bottom orbital velocity amplitude, μ_e is the lateral mixing coefficient, and ξ is the offshore distance from the mean shoreline. A value of 0.01 has been adopted for N.

In most of the previous computation of nearshore currents, constant values (on the order of 0.01) have been used for the friction coefficient C_{f}. However, since its value significantly affects the magnitude of the longshore current velocity and the resultant sediment transport rate, we should determine C_{f} in a more objective and reasonable way. Hence, in the present study, local values of C_{f} have been estimated using a frictional law of Tanaka and Shuto (1981) for a wave-current coexistent field and empirical formulas of Sato (1987) for ripple formation due to waves.

For this, first we calculate at each local point the near-bottom orbital diameter d_0 using the small-amplitude wave theory as well as the friction coefficient

f_{cw} using the frictional law, in which the presence of the longshore current is ignored and the equivalent roughness k_s is set equal to the sand grain diameter d. The empirical formulas of Sato give the critical conditions for the formation/disappearance of sand ripples and the ripple size as functions of the Shields number and d_0/d. Then we evaluate the friction coefficient C_f using the frictional law, in which this time the longshore current is included and the equivalent roughness k_s is set equal to the local ripple height, if ripples exist, or to the grain diameter d in case of no ripples. (According to previous studies, the equivalent roughness is about four times as large as the ripple height. However, the ripple height itself has been employed as k_s in this study, because the ripple crest orientation is rather parallel to the longshore current direction.) Cross-shore distributions of the longshore current velocity V_ℓ have been thus computed by iteratively solving Eq. (5) together with the frictional law for unknowns V_ℓ and C_f.

2.4 Computation of longshore sand transport rate

The sediment transport rate formula proposed by Watanabe *et al.* (1986) gives local transport rate, under general conditions of combined action of waves and currents, as the summation of the transport rate due to mean currents and that due to the direct action of waves. In the present study, by neglecting the latter, the following formula has been used for the computation of local immersed-weight rate i_ℓ of the longshore sand transport.

$$i_\ell(x) = (1 - \varepsilon_v)\, s \cdot A_c\, [\hat{\tau}_b(x) - \tau_{cr}]\, V_\ell(x) \tag{8}$$

in which ε_v and $s\ (= \rho_s/\rho - 1)$ are the porosity and the immersed specific density of the sediment, A_c is a dimensionless coefficient, $\hat{\tau}_b$ is the maximum value of the periodical bottom friction in a coexistent wave-current field, calculated by the frictional law of Tanaka and Shuto (1981) with the equivalent roughness equal to the grain diameter, τ_{cr} is the critical shear stress for the onset of general sand movement (Watanabe *et al.*, 1986), and V_ℓ is the longshore current velocity. A value of 2.0 has been adopted for the coefficient A_c on the basis of recent studies (*e.g.*, Watanabe *et al.*, 1991).

Total immersed-weight rate I_ℓ of the longshore transport has been computed by the cross-shore integration of $i_\ell(x)$:

$$I_\ell = \int_{x_0}^{\infty} i_\ell(x)\, \mathrm{d}x \tag{9}$$

where x_0 is the locations of the mean water shoreline. Then total volumetric transport rate Q_ℓ has been calculated by the following equation:

$$Q_\ell = \frac{I_\ell}{(1 - \varepsilon_v)(\rho_s - \rho)\, g} \tag{10}$$

3. Results of Computation and Discussions

3.1 Example of computation results

As one example of the results thus computed, Figure 1 shows cross-shore distributions of the wave height H, wave angle θ, longshore current velocity V_ℓ, near-bottom orbital velocity amplitude $\hat{u}_b$, immersed-weight sand transport rate i_ℓ, equivalent roughness k_s, friction coefficient C_f in the longshore current computation, and friction coefficient f_{cw} in the transport rate computation, when $d = 0.2$mm, $\tan\beta = 1/20$, $\theta_0 = 45°$, $T = 10.0$s, and $H_0 = 1.2$m.

The transport rate i_ℓ becomes maximum between the breaking point and the location of the maximum V_ℓ, as expected, not only in this case but in all the cases. The range where i_ℓ takes significant magnitude is narrower than that for V_ℓ and is comparable to the surf zone width. In the range of about 80m around the breaking point, the equivalent roughness k_s is equal to the grain size $d = 0.2$mm and hence the friction coefficients C_f and f_{cw} take common values. This is because the bottom friction in this range exceeds the critical value for the disappearance of sand ripples or the initiation of the sheet flow.

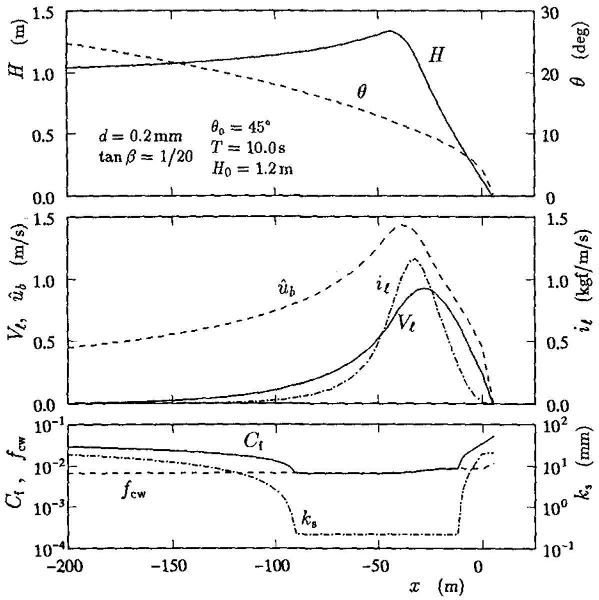

Fig. 1 Example of cross-shore distributions of computed quantities.

3.2 Total rate of longshore sand transport

First let us study the relation of the total immersed-weight transport rate I_ℓ with the longshore component of wave energy flux P_ℓ at the breaking point:

$$P_\ell = E_{\rm B}\, C_{g{\rm B}} \cdot \sin\theta_{\rm B}\, \cos\theta_{\rm B} \tag{11}$$

where $E_{\rm B}$, $C_{g{\rm B}}$ and $\theta_{\rm B}$ are the energy density, the group velocity and the wave angle of breakers. Komar and Inman (1970) have proposed the following linear relation between I_ℓ and P_ℓ on the basis of the energetics concept and field data:

$$I_\ell = 0.77\, P_\ell \tag{12}$$

in which the proportionality constant 0.77 should be halved if the energy density is calculated from the significant wave height as in the CERC formula.

Figure 2 shows a relation between I_ℓ and P_ℓ obtained in the present computation for cases of d = 0.2mm and $\tan\beta = 1/50$. The relation is remarkably independent of the incident wave period T and angle θ_0. The magnitude of I_ℓ is nearly proportional to P_ℓ under field-scale conditions, whereas it rapidly decreases under laboratory conditions, in which the maximum friction $\hat{\tau}_b$ exceeds the critical shear $\tau_{\rm cr}$ only slightly in Eq. (8). Such an overall trend is consistent with previous studies (*e.g.*, Komar and Inman, 1970).

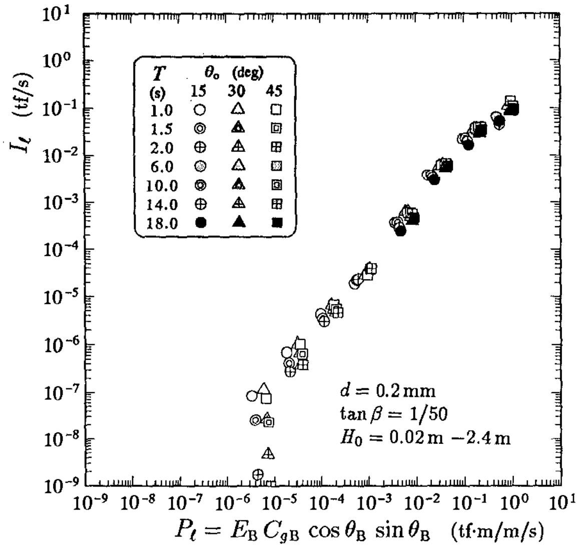

Fig. 2 Example of relation between I_ℓ and P_ℓ.

The relation between I_ℓ and P_ℓ for all the 2,520 cases is shown in Fig. 3, which indicates a trend similar to that in Fig. 2. In Fig. 3, different symbol marks are used for different grain sizes and beach slopes, but their effect on the I_ℓ-P_ℓ relation cannot be seen clearly because of the overlapping of many marks.

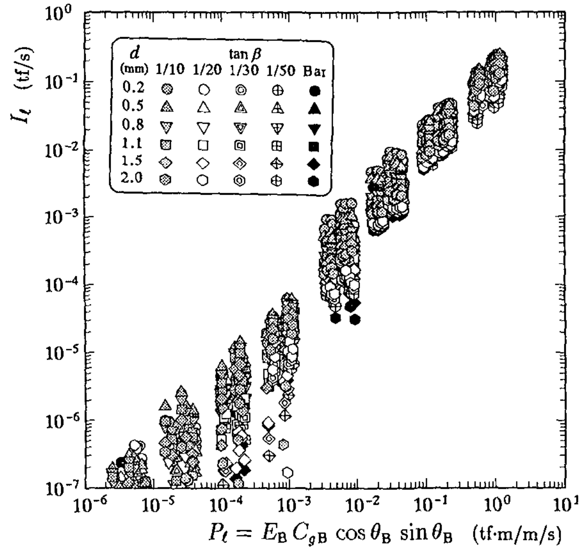

Fig. 3 Relation between I_ℓ and P_ℓ.

In order to make this clearer, we assume the linear relation, $I_\ell = \alpha_{IP} \cdot P_\ell$, for the 1,440 cases under field conditions, and calculate the proportionality coefficient α_{IP} for each grain size and bottom slope using the least-square method. Figure 4 (a) shows values of α_{IP} normalized by the mean proportionality coefficient $\overline{\alpha}_{IP}$ for all the 1,440 cases. It is seen in this figure that α_{IP} considerably decreases as the grain diameter d increases, being much less dependent on the bottom slope except for cases of $\tan\beta = 1/10$. The values of α_{IP} range between 0.04 and 0.23 with their average $\overline{\alpha}_{IP} = 0.078$, which are very much smaller than 0.77 in Eq. (12) by Komar and Inman (1970) or 0.52 proposed by Kraus *et al.* (1982), being rather close to the value of 0.06-0.12 in an empirical formula presented by Sato and Tanaka (1966). In a summary, according to the present computation, the relation between I_ℓ and P_ℓ is approximately expressed as:

$$I_\ell = (0.04 \sim 0.23)\, P_\ell \simeq 0.078\, P_\ell \tag{13}$$

For readers' information, Fig. 5 shows the relation between I_ℓ', computed by Eq. (8) with the critical shear $\tau_{cr} = 0.0$, and P_ℓ. They are proportional very well to each other not only for field-scale but also for laboratory-scale conditions.

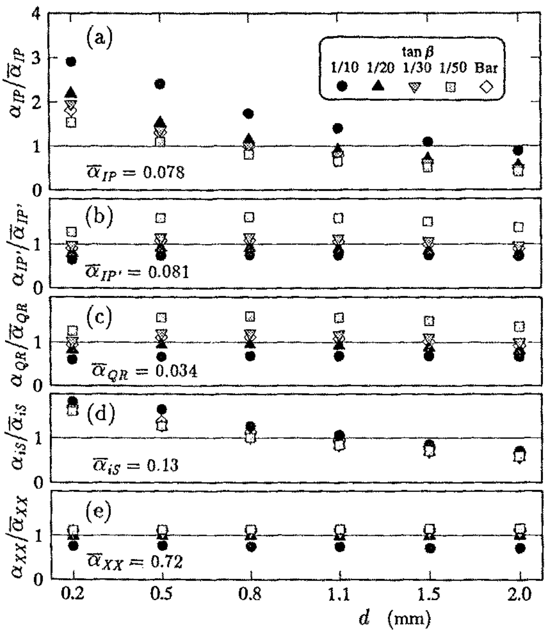

Fig. 4 Dependency of proportionality coefficients on the grain size and the beach slope.

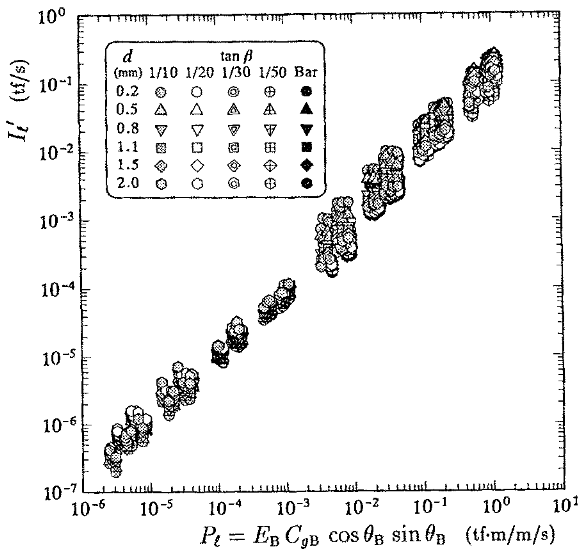

Fig. 5 Relation between I_ℓ' and P_ℓ.

Komar and Inman (1970) have reported another empirical formula based on field data as follows:

$$I_\ell = 0.28\, P_\ell' \tag{14}$$

where

$$P_\ell' = E_{\mathrm{B}}\, C_{g\mathrm{B}}\, \cos\theta_{\mathrm{B}} \cdot \overline{V}_\ell / \hat{u}_{b\mathrm{B}} \tag{15}$$

in which $\overline{V}_\ell$ is the mean velocity of the longshore current, and $\hat{u}_{b\mathrm{B}}$ is the amplitude of the near-bottom orbital velocity at the breaking point. Figure 6 shows the relation between I_ℓ and P_ℓ' in the present computation, in which $\overline{V}_\ell$ has been evaluated by simply averaging V_ℓ over the range from the breaker line to the mean shoreline. Data scattering in Fig. 6 has become small as compared to that in Fig. 3. In addition, as shown in Fig. 4 (b), the dependency of the proportionality coefficient $\alpha_{IP'}$ on the grain size and on the bottom slope is also weak except for cases of $\tan\beta = 1/50$. Values of $\alpha_{IP'}$ is still much smaller than 0.28 in Eq. (14), and the relation of the two quantities is expressed as:

$$I_\ell = (0.05 \sim 0.13)\, P_\ell' \simeq 0.08\, P_\ell' \tag{16}$$

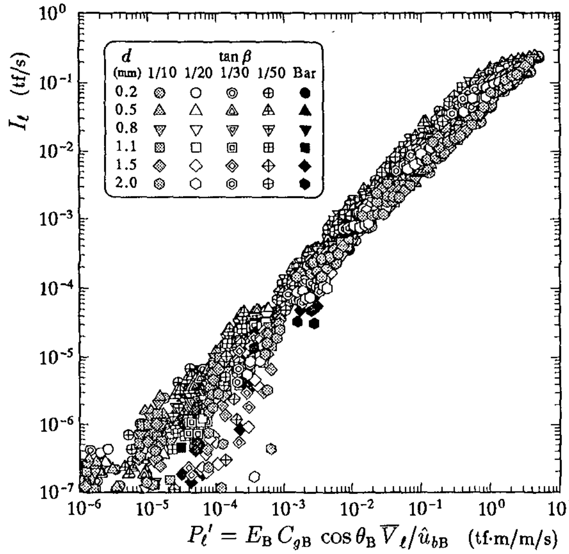

Fig. 6 Relation between I_ℓ and P_ℓ'.

In order that the relation $I_\ell \propto P_\ell \propto P_\ell'$ holds good, the mean longshore current velocity $\overline{V}_\ell$ must be proportional to $\hat{u}_{b\mathrm{B}} \cdot \sin\theta_{\mathrm{B}}$. Their relation is shown in Fig. 7. Although these two quantities approximately satisfy a proportional relation for an individual combination of the grain diameter d and the bottom slope $\tan\beta$, values of the proportionality coefficient change over the range of one-order of magnitude, depending on d and $\tan\beta$.

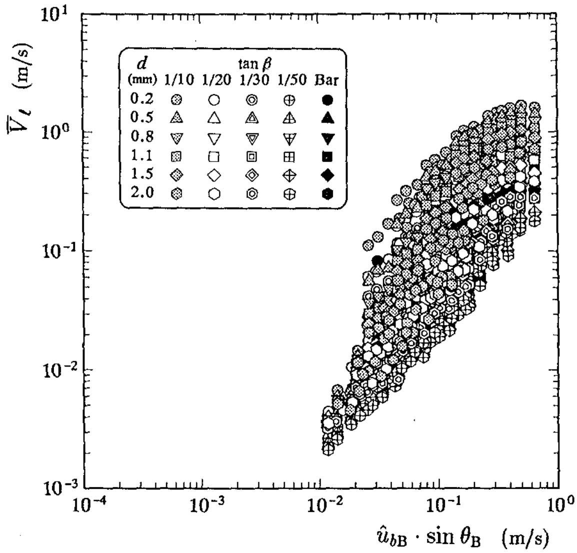

Fig. 7 Relation between $\overline{V}_\ell$ and $\hat{u}_{bB} \cdot \sin\theta_B$.

Now let us make the following long wave approximation:

$$\left.\begin{aligned} C_{gB} &\simeq \sqrt{gD_B}, \quad \cos\theta_B \simeq 1 \\ \hat{u}_{bB} &\simeq (H_B/2)\sqrt{g/D_B} \simeq (\gamma/2)\sqrt{gD_B} \end{aligned}\right\} \tag{17}$$

for the parameter $P_\ell{}'$ defined by Eq. (15). Then we obtain the relation:

$$P_\ell{}' \simeq (\rho g/4\gamma)\, H_B^2 \overline{V}_\ell \tag{18}$$

where γ is the ratio of the wave height H_B to the mean depth D_B, and is practically constant. Hence we can expect a linear relation between the total volumetric transport rate Q_ℓ and a new parameter R_ℓ defined as:

$$R_\ell = H_B^2\, \overline{V}_\ell \tag{19}$$

which is consistent in the dimension with Q_ℓ. The relation between Q_ℓ and R_ℓ is shown in Fig. 8. As expected, for the field-scale conditions, Q_ℓ is approximately proportional to R_ℓ as expressed by the following relation (See Fig. 4 (c)):

$$Q_\ell = (0.020 \sim 0.053)\, R_\ell \simeq 0.034\, R_\ell \tag{20}$$

It is interesting (and strange in a sense) that the value of 0.034 of the mean proportionality coefficient in Eq. (20) is very close to 0.024 in the empirical formula presented by Kraus *et al.* on the basis of field data, because using the same data set they have obtained the value of 0.52 as the proportionality constant in the I_ℓ-P_ℓ relation, which is very much larger than the value of 0.078 in Eq. (13).

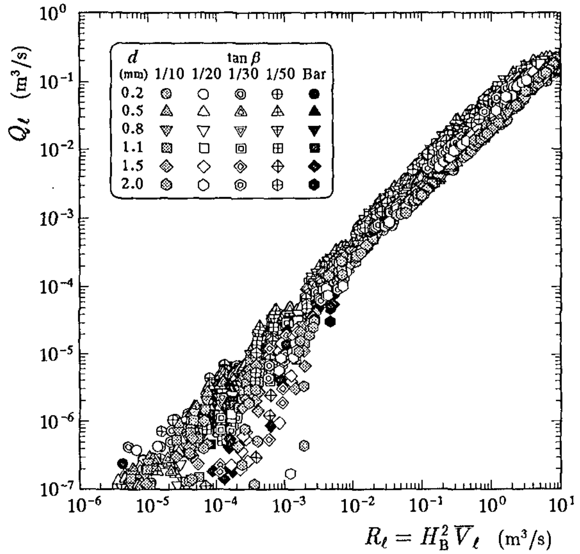

Fig. 8 Relation between Q_ℓ and R_ℓ.

3.3 Cross-shore distribution of longshore transport rate

As described in 3.1 in reference to Fig. 1, the local rate of the longshore transport i_ℓ becomes maximum between the breaking point and the location of the maximum longshore current velocity, and takes significant values over a range as wide as the surf zone. However, since the cross-shore distributions of i_ℓ may not necessarily be similar for various conditions of the grain size, bottom slope and incident waves, it seems difficult to express them in a single normalized form. Hence here we will examine only the magnitude of the maximum local transport rate $i_{\ell\max}$ and the offshore distance $X_{i\ell\max}$ of the point of $i_{\ell\max}$, which are regarded as the most important representative parameters in the cross-shore distributions of i_ℓ.

First, concerning the maximum transport rate $i_{\ell\max}$, since the total rate I_ℓ is approximately proportional to P_ℓ and the width of the significant longshore transport zone is comparable with the surf zone width X_B (the distance between the breaking point and the mean shoreline), $i_{\ell\max}$ may be related to a parameter $S_\ell = P_\ell/X_B$. As expected, it is seen in Fig. 9 that a fairly high correlation exists between $i_{\ell\max}$ and S_ℓ. According to Fig. 4 (d), the value of the proportionality coefficient $\alpha_{iS} = i_{\ell\max}/S_\ell$ obtained for the field-scale cases decreases as the grain size increases, being nearly independent of the bottom slope. Under the field-scale conditions, the relation between these two parameters is expressed as:

$$i_{\ell\max} = (0.075 \sim 0.24)\, S_\ell \simeq 0.13\, S_\ell \tag{21}$$

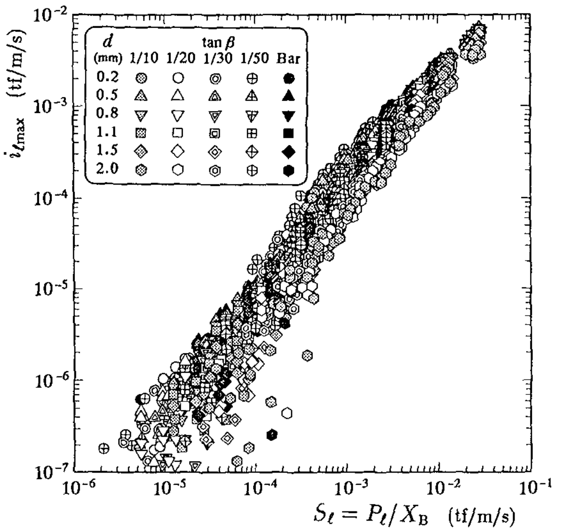

Fig. 9 Relation between $i_{\ell\max}$ and S_ℓ.

Then the relation between $X_{i\ell\max}$ (the offshore distance of the point of $i_{\ell\max}$ measured from the mean shoreline) and X_B is shown in Fig. 10, where plotted are points more than 2,300 except for the data with $i_{\ell\max} < 10^{-7}$ tf/m/s. The two parameters show such a remarkably highly proportional relation that only a small number of points can be seen because of their overlapping. According to this figure as well as Fig. 4 (e), the proportionality coefficient $\alpha_{XX} = X_{i\ell\max}/X_B$ takes nearly constant values depending very weakly on the grain size and the bottom slope. The relation is expressed as:

$$X_{i\ell\max} = (0.52 \sim 0.83)\, X_B \simeq 0.72\, X_B \tag{22}$$

4. Concluding Remarks

Major conclusions of this study are as follows:

(1) The validity of the local transport rate formula and that of the conventional total rate formulas for the longshore transport have been reinforced each other at least qualitatively.

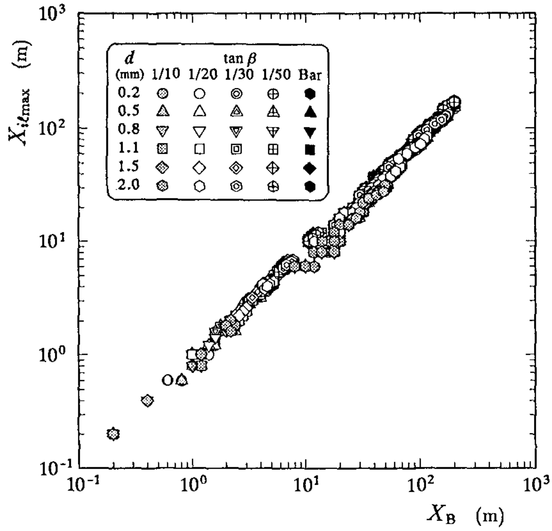

Fig. 10 Relation between $X_{i\ell\mathrm{max}}$ and X_{B}.

(2) Under the field-scale conditions, the total immersed-weight transport rate I_ℓ is approximately proportional to the longshore wave power component P_ℓ. However, the value of the proportionality coefficient obtained in this study is very much smaller than 0.77 in Komar and Inman's formula and is rather close to the value in Sato and Tanaka's formula, decreasing as the grain size increases. It should be noted that in many examples of the actual application of the I_ℓ-P_ℓ formula to one-line models, values between 0.05 and 0.4 have been adopted for the coefficient on the basis of the calibration using past beach change data.

(3) Under the laboratory-scale conditions, the effect of the critical shear stress τ_{cr} cannot be neglected.

(4) I_ℓ and P_ℓ' as well as Q_ℓ and R_ℓ have also shown a highly proportional relation, respectively, particularly under the field-scale conditions. The proportionality coefficients are weakly dependent on the grain size.

(5) Concerning the cross-shore distributions of the longshore transport rate, it has been found that $i_{\ell\mathrm{max}}$ and S_ℓ as well as $X_{i\ell\mathrm{max}}$ and X_{B} are also proportional to each other.

Further study should be conducted on the effects of the beach profiles (more realistic profiles, other than uniform slopes, corresponding to given conditions of sediment grain size and incident waves), breaker-induced turbulent stresses, grain size distributions, effective bottom roughness, beach transport in the swash zone, random waves, and so on.

REFERENCES

Komar, P.D. and D.L. Inman (1970): Longshore sand transport on beaches, *Jour. Geophys. Res.*, Vol. 75, No. 30, pp. 5914-5927.

Kraus, N.C., M. Isobe, H. Igarashi, T.O. Sasaki and K. Horikawa (1982): Field experiments on longshore sand transport in the surf zone, *Proc. 18th Coastal Eng. Conf.*, ASCE, pp. 969-988.

Nishimura, H. (1988): Computation of Nearshore Current, in *Nearshore Dynamics and Coastal Processes* (edited by K. Horikawa), Part. III, Chap. 3, University of Tokyo Press, pp. 272-273.

Sato, S. and N. Tanaka (1966): Field investigation on sand drift at Port Kashima facing the Pacific Ocean, *Proc. 10th Coastal Eng. Conf.*, ASCE, pp. 595-614.

Sato, S. (1987): Oscillatory Boundary Layer Flow and Sand Movement over Ripples, *Doctoral Dissertation*, Univ. of Tokyo, 138p.

Tanaka, H. and N. Shuto (1981): Friction coefficient for a wave-current coexistent system, *Coastal Eng. in Japan*, JSCE, Vol. 24, pp. 105-128.

Watanabe, A., T. Hara and K. Horikawa (1984): Study on breaking condition for compound wave trains, *Coastal Eng. in Japan*, JSCE, Vol. 27, pp. 71-82.

Watanabe, A. and K. Maruyama (1986): Numerical modeling of nearshore wave field under combined refraction, diffraction and breaking, *Coastal Eng. in Japan*, JSCE, Vol. 29, pp. 19-39.

Watanabe, A., K. Maruyama, T. Shimizu and T. Sakakiyama (1986): Numerical prediction model of three-dimensional beach deformation around a structure, *Coastal Eng. in Japan*, JSCE, Vol. 29, pp. 179-194.

Watanabe, A., T. Shimizu and K. Kondo (1991): Field application of a numerical model of beach topography change, *Proc. Coastal Sediments '91*, ASCE, pp. 1814-1828.

Watanabe, A. and M. Dibajnia (1988): A numerical model of wave deformation in surf zone, *Proc. 21st Coastal Eng. Conf.*, ASCE, pp. 578-587.